CHAPTER II
LITERATURE REVIEW

2.1 Photocatalytic Reaction

In recent years, numerous studies have been reported on the photocatalytic detoxification by using semiconductor particles as photocatalysts such as TiO_2, ZnO, Fe_2O_3. Among the semiconductor employed, TiO_2 is extensively used photocatalytic. It is known as inexpensive, nontoxic and very effective semiconductor photocatalysts (Herrmann, 1999).

2.1.1 Principle of Photocatalytic

The initial process for photocatalytic reaction is occurred when a photon is absorbed by a semiconductor material that promotes an electron (e^-) from the valence band to the conduction band, creating an electronic vacancy or "hole" (h^+) at the valence band edge (Fox *et al.*, 1993) The hole is a very powerful oxidizing agent and is capable of oxidizing a variety of organic molecules as well as generating hydroxyl radicals as shown in the Figure 2.1 Upon excitation, the fate of the separated electron and hole can follow several pathways. Figure 2.2 illustrates some of the deexcitation pathways for the electrons and holes. (Linsebigler *et al.*, 1995)

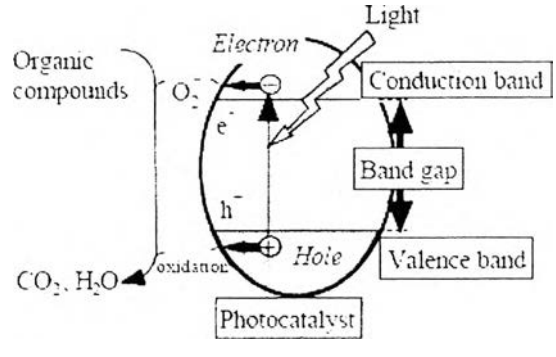

Figure 2.1 The excitation of an electron from the valence band to the conduction band initiated by light absorption with energy equal to or greater than the band gap of the semiconductor.

Thus in concert, electron and hole pair (e^--h^+) is generated. The following chain reactions have been widely postulated reactions (Eqs. (1.1) – (1.6) as follows: (Gaya *et al.*, 2008)

$$\text{Photoexcitation: Semiconductor} + h\upsilon \rightarrow e^- + h^+ \quad (1.1)$$

$$\text{Oxygen ionosorption: } (O_2)_{ads} + e^- \rightarrow O_2^{\bullet -} \quad (1.2)$$

$$\text{Ionization of water: } H_2O \rightarrow OH^- + H^+ \quad (1.3)$$

$$\text{Protonation of superoxides: } O_2^{\bullet -} + H^+ \rightarrow HOO^{\bullet} \quad (1.4)$$

The hydroperoxyl radical formed in (1.4) also has scavenging property as O_2 thus doubly prolonging the lifetime of photohole:

$$HOO^{\bullet} + e^- \rightarrow HO^{2-} \quad (1.5)$$

$$HOO^- + H^+ \rightarrow H_2O_2 \quad (1.6)$$

Both the oxidation and reduction can take place at the surface of the photoexcited semiconductor photocatalyst (see Figure 2.2). Recombination between electron and hole occurs unless oxygen is available to scavenge the electrons to form superoxides ($O_2^{\bullet -}$), its protonated form the hydroperoxyl radical ($HO_2^{\bullet}$) and subsequently H_2O_2.

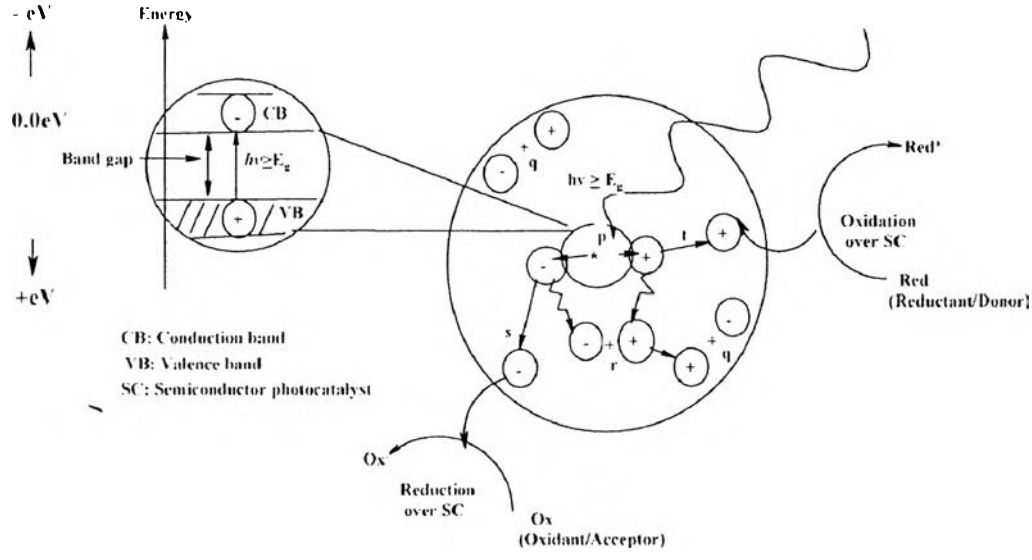

Figure 2.2 Schematic photophysical and photochemical processes over photon activated semiconductor cluster (p) photogeneration of electron/hole pair, (q) surface recombination,(r) recombination in the bulk, (s) diffusion of acceptor and reduction on the surface of Semiconductor (SC), and (t) oxidation of donor on the surface of SC particle.

2.2 TiO_2 Photocatalytic Reaction

2.2.1 Mechanism of TiO_2 Photocatalysis

When photocatalyst titanium dioxide (TiO_2) absorbs ultraviolet (UV) radiation, it will produce pairs of electrons and holes. The electron of the valence band of TiO_2 becomes excited when illuminated by light. The excess energy of this excited electron promoted the electron to the conduction band of TiO_2 thereby creating the negative-electron (e^-) and positive-hole (h^+) pair. The photonic excitation leaves behind an empty unfilled valence band, and thus creating the electron-hole pair (e^-–h^+). The series of chain oxidative–reductive reactions (Eqs. (1.7) – (1.17) that occur at the photon activated surface was vastly supposed as follows: (Chong *et al.*, 2010)

Photoexcitation: $TiO_2 + h\nu \rightarrow e^- + h^+$ (1.7)

Charge-carrier trapping of e^-: $e^-_{CB} \rightarrow e^-_{TR}$ (1.8)

Charge-carrier trapping of h^+: $h^+_{VB} \rightarrow h^+_{TR}$ (1.9)

Electron-hole recombination: $e^-_{TR} + h^+_{VB}(h^+_{TR}) \rightarrow e^-_{CB}$ + heat (1.10)

Photoexcited e^- scavenging: $(O_2)_{ads} + e^- \rightarrow O_2^{\bullet -}$ (1.11)

Oxidation of hydroxyls: $OH^- + h^+ \rightarrow OH^\bullet$ (1.12)

Photodegradation by $OH^\bullet$: $R\text{–}H + OH^\bullet \rightarrow R'^\bullet + H_2$ (1.13)

Direct photoholes: $R + h^+ \rightarrow R^{+\bullet} \rightarrow$Intermediate(s)/Final Degradation Products (1.14)

Protonation of superoxides: $O_2^{\bullet -} + OH^\bullet \rightarrow HOO^\bullet$ (1.15)

Co-scavenging of e^-: $HOO^\bullet + e^- \rightarrow HO_2^-$ (1.16)

Formation of H_2O_2: $HOO^- + H^+ \rightarrow H_2O_2$ (1.17)

Essentially, hydroxyl radicals ($^\bullet OH$), holes (h^+), superoxide ions (O_2^-) and hydroperoxyl radicals ($^\bullet OOH$) are highly reactive intermediates that will act concomitantly to oxidize large variety of organic pollutants including volatile organic compounds (VOCs) (Jacoby *et al.*, 1996) and bioaerosols as equation below and Figure 2.3(Herrmann, 1999).

$$\text{Organic contaminant} \xrightarrow[\text{ii) } O_2 \quad \text{iii) } h\nu \geq E_g]{\text{i) } TiO_2} \text{Intermediate(s)} \longrightarrow CO_2 + H_2O + HA$$

Chong *et al.*, (2010) depicts the mechanism of the electronehole pair formation when the TiO_2 particle is irradiated with adequate *hv*. The light wavelength for such photon energy as shown in Figure 2.3.

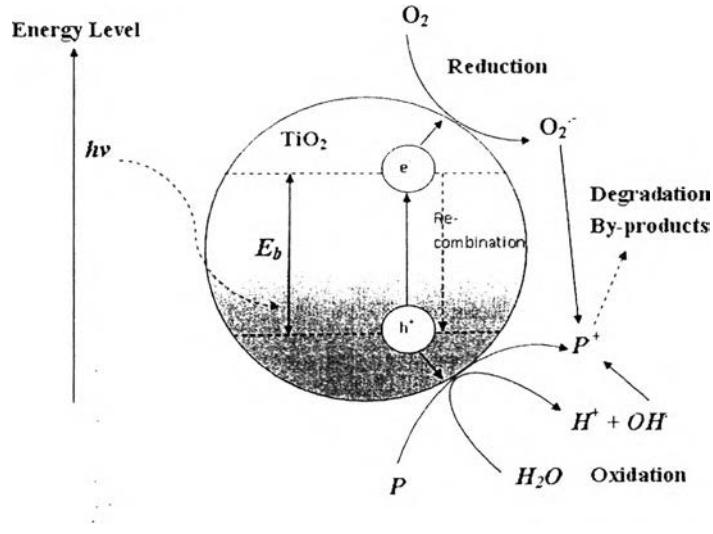

Figure 2.3 Photo-induced formation mechanism of electron–hole pair in a semiconductor TiO_2 particle with the presence of pollutant (P).

The energy difference between the valence band and conduction band is known as "Band gap" Wavelength of the light necessary for photo-excitation (Kathirvelu *et al.*, 2008).

The energy of a photon (E) depends only on its frequency (v) or equivalently, its wavelength (λ):

$$E = h\nu = hc/\lambda$$

Where h is Planck's constant = 6.625×10^{-34} JS^{-1}

λ is wavelength

c is velocity of light = 3×10^8 m/s

The band gap energy of TiO_2 = 3.2 eV (Linsebigler *et al.*, 1995) as shown in Figure 2.4.

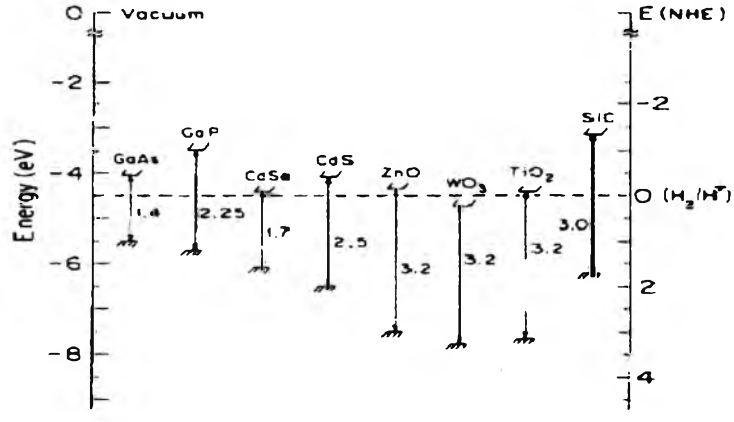

Figure 2.4 The variation in the energy gap between different semiconductors.

Accordingly, Wavelength of photon which has energy equal band gap energy of TiO_2 can calculate as illustrated from equation below equals to 388 nm (UVA).

$$\lambda = \frac{hc}{\varepsilon}$$

$$\lambda = \frac{(6.625 \times 10^{-34}\ \text{J - s}) \times (3 \times 10^{8}\ \text{m/s})}{3.2\text{eV}} \times \frac{1\text{eV}}{1.6 \times 10^{-19}\ \text{J}}$$

$$= 0.388 \times 10^{-6}\ \text{m} \quad \text{or} \quad 0.388\ \mu\text{m} \quad \text{or} \quad 388\ \text{nm}$$

2.2.2 Strategies to Ameliorate the Photocatalytic Activity of TiO_2

Zhang *et al.*, (1998) reported that particle size is a crucial factor in the dynamics of the electron/hole recombination process

Xu *et al.*, (1999) suggested that Photocatalytic activity of TiO_2 also increased as the particle size of TiO_2 became smaller, especially when the particle size is less than 30 nm The half-life ($t_{0.5}$) of the photocatalytic degradation of methylene blue also decreased as the particle sizes of TiO_2 decreased. Besides, increase the surface-to-volume ratio of anatase particles. (Kim *et al.*, 2007).

Thus, the design and preparation of TiO_2 nanorods or nanofibers has attracted great attention because of their potential for enhancing photocatalytic activity with high surface area. Using different methods, To illustrate Chuangchote *et al.*, (2009) report herein a simple procedure for the fabrication of TiO_2 nanofibers by

the combination of electrospinning and sol–gel techniques by using poly(vinylpyrrolidone) (PVP), titanium(IV) butoxide, and acetylacetone in methanol as a spinning solution. TiO_2 nanofibers (260–355 nm in diameter), with a bundle of nanofibrils (20–25 nm in diameters) aligned in the fiber direction, However Klimisch *et al.*, (1997) reported that vinyl pyrrolidone monomer is carcinogen and Electrospinning apparatus (see Figure 2.5) price is still high

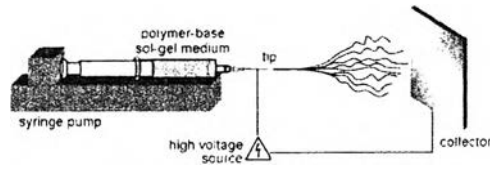

Figure 2.5 Electrospinning apparatus.

Sun *et al.*, (2009) used Bacterial cellulose as a supporting catalyst to replace synthetic polymers and reported that Bacterial cellulose nanofibers were biosynthesized by *Acetobacter xylinum* and displayed a remarkable capability for orienting TiO_2 nanoparticle arrays.

2.2.3 Applications of TiO_2 Photocatalytic

2.2.3.1 Self Cleaning Property

Kiwi *et al.*, (2010) reported that Nanocrystalline anatase TiO_2 with small particles size distribution was synthesized and subsequently loaded on cotton that good reproducibility for the discoloration was obtained in both cases for red wine stains under simulated solar light as shown in Figure 2.6 and they suggested mechanism Self cleaning of TiO_2 photocatalytic as illustrated in Figure 2.7

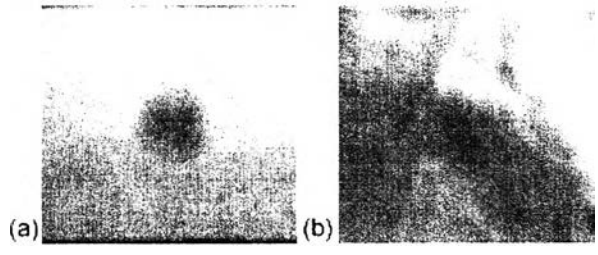

Figure 2.6 Discoloration of wine stains on TiO_2–cotton: pretreated by RF for 10 min no vacuum (a) before and (b) after Suntest irradiation.

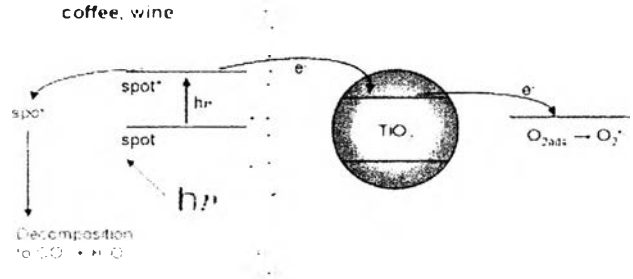

Figure 2.7 Scheme of the self-cleaning mechanism of wine pigments on TiO_2-cotton.

2.2.3.2 Pollutant Photodegradation Property

Mill *et al.*, (1997) illustrated mechanism of photodegradation pollutant by TiO_2 as shown in Figure 2.8

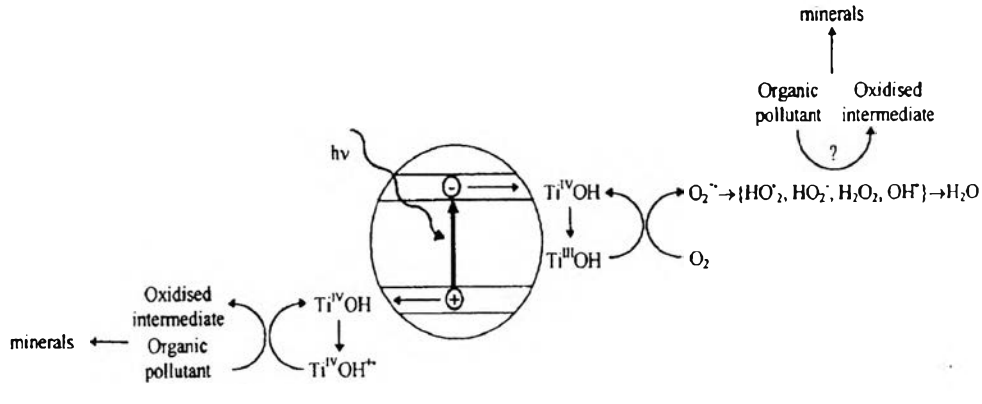

Figure 2.8 Mechanism of photodegradation pollution by TiO_2.

Vulliet *et al.*, (2002) reported that The photocatalytic degradation of two sulfonylurea herbicides (cinosulfuron and triasulfuron) in aqueous solutions was studied using TiO_2 as a catalyst. The quantum efficiencies were identical for both herbicides (0.73%). All the results presented show that this process could be efficiently used in the field of agricultural water decontamination.

Konstantinou *et al.*, (2003) reported that Effective destruction of various pesticides belonging to different chemical families e.g. Organophosphorous, Carbamate, Organochlorin, Chlorophenol pesticides, etc. is possible by photocatalysis in the presence of TiO_2 suspensions.

Chatterjee *et al.*, (2006) reported that Visible light assisted photodegradation of various halocarbons, viz. chloro-phenols, trichloroethylene, 1,2-dichloroethane and 1,4-dichlorobenzene, has been achieved on the surface of dye-modified TiO_2 semiconductor.

Bianchi *et al.*, (2009) reported that N-doped TiO_2 samples prepared from $TiCl_3$ salt solution as TiO_2 source and ammonia solution as Nitrogen source at pH 9 degrade Toluene 79.6 %.

Bansal *et al.*, (2010) reported that C.I. acid orange 7 Azo dye which represent the largest class of dyes used in textile-processing and other industries could be successfully decolorized and degraded by titania based photocatalysis.

2.2.3.3 Antibacterial Property

Kim *et al.*, (2003) reported that in the photocatalytic bactericidal effect on food pathogenic bacteria, it was confirmed that both near-UV illumination time and TiO_2 concentrations affected the cell killing activity. UV illumination time affected drastically the viability of all bacteria with different death rate. Similar trends were obtained from *Salmonella choleraesuis* subsp. and *Vibrio parahaemolyticus* that their complete killing was achieved after 3 h of illumination. However, *Listeria monocytogenes* was more resistant and its death ratio was about 87% at that time as demonstrated as Figure 2.9

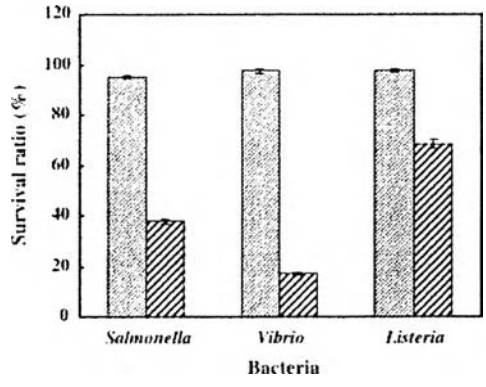

Figure 2.9 Comparison of cell viability with difference bacteria at TiO_2 concentration (1 mg/ml) and near-UV illumination time 30 min. (▨ , only UV light; ▨ , UV + TiO_2 1.00 mg/ml).

Sunada *et al.*, (2003) reported that the process of *E. coli* photokilling on TiO_2 film. The initial reaction is a partial decomposition of the outer membrane by the reactive species produced by TiO_2 photocatalysis, Correspondingly, the permebility change of the outer membrane enables reactive species to easily reach the cytoplasmic membrane. Thus, the cytoplasmic membrane is attacked by reactive species, leading to the peroxidation of membrane lipid. Thus, the structural and functional disorders of the cytoplasmic membrane that is the root of the killing effect by TiO_2 photocatalysis can be schematically illustrated as in Figure 2.10.

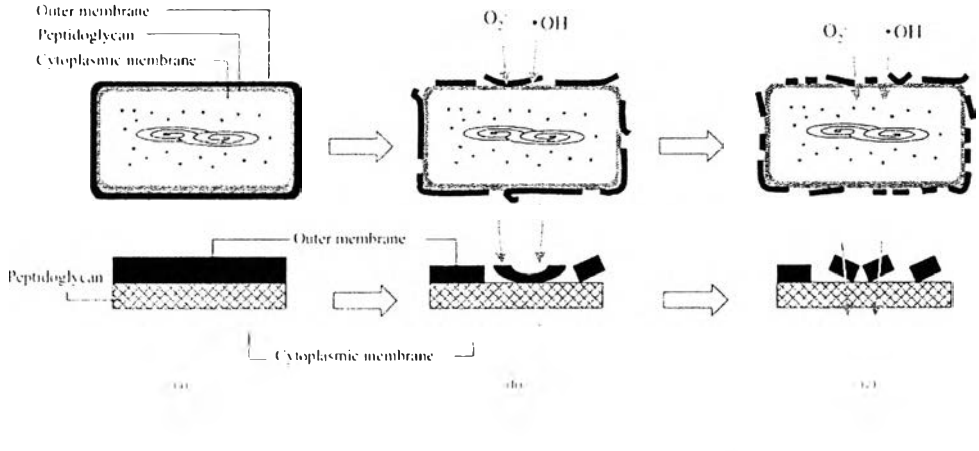

Figure 2.10 The process of *E. coli* photokilling on TiO_2 film.

Fujishima *et al.*, (2000) summarize application of Titanium dioxide photocatalysis as manifest in Table 2.1.

Table 2.1 Selected applications of photocatalysis

Property	Category	Application
Self-cleaning	Materials for residential and office buildings	Exterior tiles, kitchen and bathroom components, interior furnishings, plastic surfaces, aluminum siding, building stone and curtains, paper window blinds
	Indoor and outdoor lamps and related systems	Translucent paper for indoor lamp covers, coatings on fluorescent lamps and highway tunnel lamp cover glass
	Materials for roads	Tunnel wall, soundproofed wall, traffic signs and reflectors
	Others	Tent material, cloth for hospital garments and uniforms and spray coatings for cars
Air cleaning	Indoor air cleaners	Room air cleaner, photocatalyst-equipped air conditioners and interior air cleaner for factories
	Outdoor air purifiers	Concrete for highways, roadways and footpaths, tunnel walls, soundproof walls and building walls
Water purification	Drinking water	Raw water, ground water, lakes and water-storage tanks
	Others	Fish feeding tanks, drainage water and industrial wastewater
Antitumor activity	Cancer therapy	Endoscopic-like instruments
Self-sterilizing	Hospital	Tiles to cover the floor and walls of operating rooms, silicone rubber for medical catheters and hospital garments and uniforms
	Others	Public rest rooms, bathrooms and rat breeding rooms

2.3 Bacterial Cellulose (BC)

2.3.1 Introduction of BC

Cellulose (see Figure 2.11) is the most abundant biopolymer on earth, recognized as the major component of plant biomass (Astley el al., 2001), but also a representative of microbial extracellular polymers. Bacterial cellulose belongs to specific products of primary metabolism and is mainly a protective coating. (Geyer *et al.*, 1994) as shown in Figure 2.12.

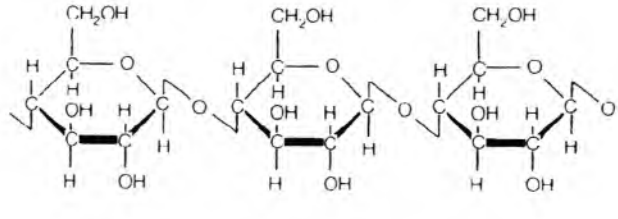

Figure 2.11 Chemical Structure of cellulose.

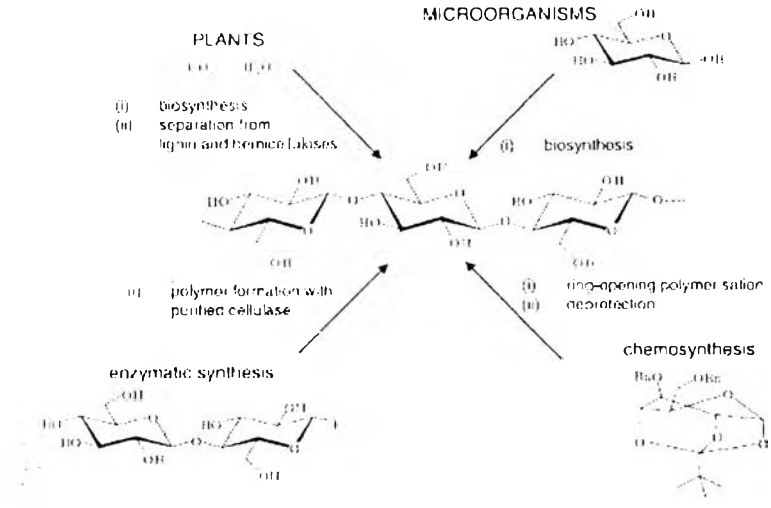

Figure 2.12 The pathways to form the biopolymer cellulose from plants or microorganism.

Cellulose is synthesized by bacteria (Table 2.2) belonging to the genera *Acetobacter*, *Rhizobium*, *Agrobacterium*, and *Sarcina* (Jonas and Farah, 1998).

Table 2.2 Bacterial cellulose producers (Jonas and Farah, 1998)

Genus	Cellulose structure
Acetobacter	extracellular pellicle composed of ribbons
Achromobacter	fibrils
Aerobacter	fibrils
Agrobacterium	short fibrils
Alcaligenes	fibrils
Pseudomonas	no distinct fibrils
Rhizobium	short fibrils
Sarcina	amorphous cellulose
Zoogloea	not well defined

Klemm *et al.*, (2001) reported that The most efficient producers are Gram-negative, acetic acid bacteria *Acetobacter xylinum* .

Geyer *et al.*, (1994) reported that *Acetobacter xylinum* produces highly crystalline cellulose extracellularly using glucose as a carbon source. The polymer formed is free of other biogenic compounds, separable in a simple way and characterized by its high water-absorption capacity as shown in Figures 2.13 and 2.14.

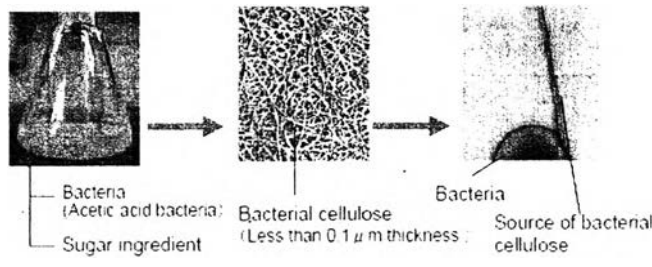

Figure 2.13 Cellulose is synthesized by Acetic acid bacteria.

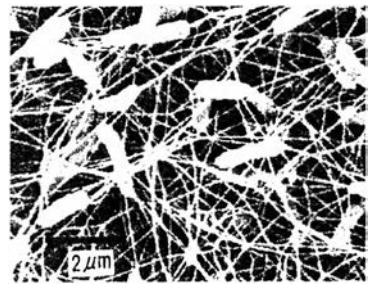

Figure 2.14 A scanning electron micrograph of freeze-dried surface of bacterial cellulose with *Acetobacter xylinum*.

Intensive studied on Bacterial cellulose synthesis, using *A. xylinum* as a model bacterium, were started by Hestrin *et al.*, (1954), who proved that resting and lyophilized *Acetobacter* cells synthesized cellulose in the presence of glucose and oxygen. By Culture methods: The source substance of bacterial cellulose is saccharides. A typical culture medium widely of use in laboratories is prepared by

dissolving, 50 g sucrose, 5 g yeast-extract, 5 g $(NH_4)_2SO_4$, 3 g KH_2PO_4, and 0.05 g $MgSO_4 \cdot 7H_2O$ in a litre of water

Yoshinaga *et al.*, (1997) reported that the molecular formula of Bacterial cellulose $(C_6H_{10}O_5)_n$, having a β-1,4 linkage between two glucose molecules and Hydrogen bonding as illustrated in Figures 2.15 and 2.16.

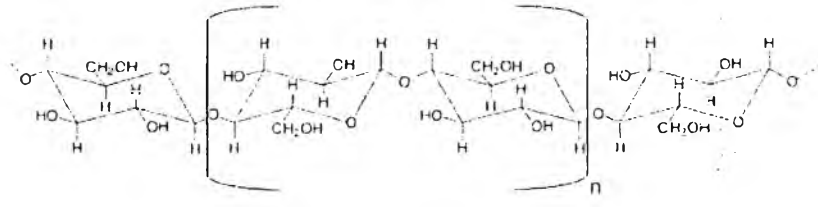

Figure 2.15 The chemical structure of the β-(1,4)-glucan chains in cellulose.

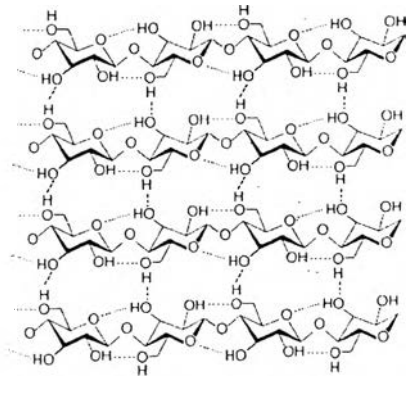

Figure 2.16 The hydrogen bonds within and between cellulose molecules.

Bielecki *et al.*, (2005) reported that *A. xylinum* cellulose consists of ribbons of microfibrils generated at the surface of the bacterial cell. The dimensions of the ribbons are 3–4 nm thick and 70–80 nm wide. The shape of microbial cellulose sheet seems to be maintained by hydrophobic bonds. It is reported that in the course of time inter- and intramolecular hydrogen bonds initially occur in each cellulose sheet, and then the cellulose crystalline structure is formed with the development of hydrogen bonds between cellulose sheets.

Czaja *et al.*, (2005) 3-D structure consisting of an ultrafine network of Bacterial cellulose nanofibres (3–8 nm) which are highly uniaxially oriented, not found in vascular plant cellulose, results in high cellulose crystallinity (60–80%) and an enormous mechanical strength. Particularly impressive is the fact that the size of microbial cellulose fibrils is about 100 times smaller than that of plant cellulose as shown in Figure 2.17.

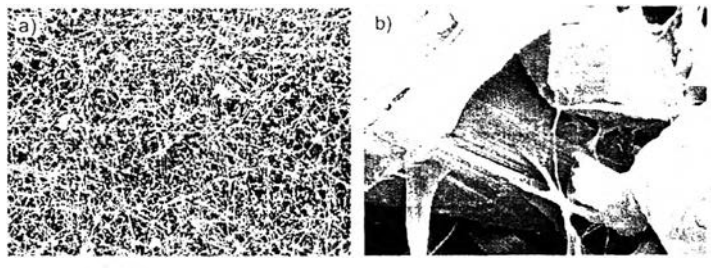

Figure 2.17 A comparison of microfibrillar organization between *Acetobacter* cellulose (a) and wood pulp (b) (both at 5000x).

Yamanaka *et al.*, (1989) reported that morphologically, fibrils in the sheets appear to constitute a pile of thin layers, as seen in Figure 2.18.

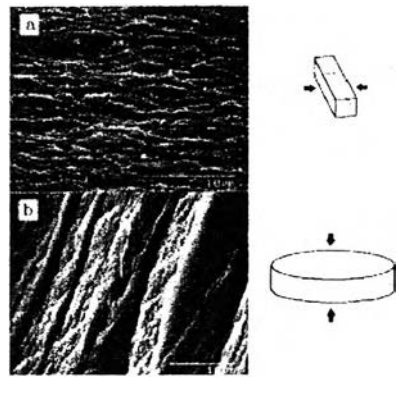

Figure 2.18 Scanning electron-micrographs of (a) cross-section and (b) surface of bacterial cellulose film.

2.3.2 Properties of Bacterial Cellulose

Shoda and Sugano, (2005) reported that Bacterial cellulose (BC) is preferred over the plant cellulose as it can be exhibits the following unique properties:

(i) High purity, as neither hemicellulose nor lignin in plant cellulose is present.

(ii) High crystallinity

(iii) BC-sheets form, high Young's modulus of 15~30 GPa, the highest of all the two-dimensional organic materials

(iv) Excellent biodegradability

(v) Large water holding capacity, upto one hundred times its weight

(vi) Excellent biological affinity

Iguchi *et al.*, (1988) reported that the mechanical properties of bacterial cellulose films prepared in Heat-press condition shown in Table 2.3.

Table 2.3 Mechanical properties of bacterial cellulose films prepared in Heat-press conditions

Culture time/(days)	7
Preparation method	Heat-press[a]
Temperature/ °C	150
Pressure/(kPa)	49
Film thickness/μm	< μm
Young's modulus/GPa	16.9
Tensile strength/MPa	260
Elongation/%	2.1

[a] Press direction: normal to the plane of growth

Henriksson *et al.*, (2008) reported that the stress–strain curves for Bacterial cellulose (BC) films molded under different compression pressures are shown in Figure 2.19.

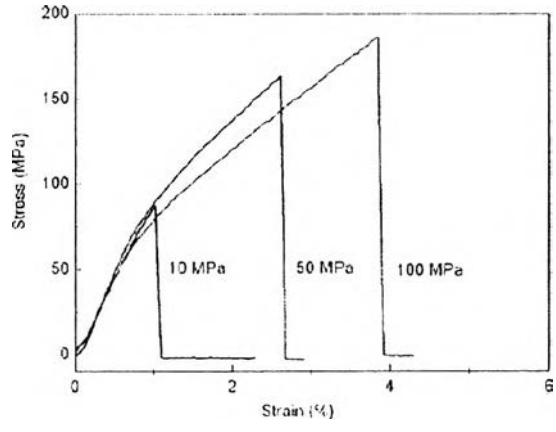

Figure 2.19 Stress–strain curves for BC films obtained under different mold compression pressures.

2.3.3 Applications of Bacterial Cellulose

2.3.3.1 Food Applications

Chawla *et al.*, (2009) reported that chemically pure cellulose can be used in processed foods as thickening and stabilizing agent. The first use of microbial cellulose in the food industries was in nata de coco in the Philippines. In 1992, microbial cellulose was introduced into diet drinks in Japan. Acetobacter was grown along with yeast in the tea extract and sugar.

2.3.3.2 Medical Applications

Microbial cellulose has high tensile strength, high porosity and microfibrillar structure. Chronic wounds such as venous leg ulcers, bedsores, and diabetic ulcers are difficult to heal, and they represent a significant clinical challenge both for the patients and for the healthcare professionals (Chawla *et al.*, 2009).

Maneerung *et al.*, (2008) reported that Bacterial cellulose is an interesting material for using as a wound dressing since it provides moist environment to a wound resulting in a better wound healing. Besides, the freeze-dried silver nanoparticle-impregnated bacterial cellulose exhibited strong the ant microbial activity against *Escherichia coli* (Gram-negative) and *Staphylococcus aureus* (Gram-positive).

Klemm *et al.*, (2001) reported that Bacterial cellulose is high mechanical strength in wet state, enormous water retention values, low roughness of the inner surface, and a complete 'vitalization' of BASYC® — microvessel-interpositions in rat experiments demonstrate the high potential of BASYC® as an artificial blood vessel in microsurgery as shown in Figure 2.20.

Figure 2.20 Application of the BASYC ®- tube in microsurgery as artificial blood.

2.3.3.3 Non-Medical Applications

The unique physical and mechanical properties of microbial cellulose such as high reflectivity, flexibility, light mass and ease of portability, wide viewing angles, and its purity and uniformity determine the applications in the electronic paper display (Chawla *et al.*, 2009).

Legnani *et al.*, (2008) reported that Bacterial cellulose (BC) membranes produced by gram-negative, acetic acid bacteria (*Gluconacetobacter xylinus*), were used as flexible substrates for the fabrication of Organic Light Emitting Diodes (OLED).

Sun *et al.*, (2010) reported that Bacterial cellulose (BC) displayed a remarkable capability for orienting TiO_2 nanoparticle arrays. Large quantities of uniform BC nanofibers coated with TiO_2 nanoparticles can be easily prepared by surface hydrolysis with molecular precision, resulting in the formation of uniform and well-defined hybrid nanofiber structures as shown in Figure 2.21.

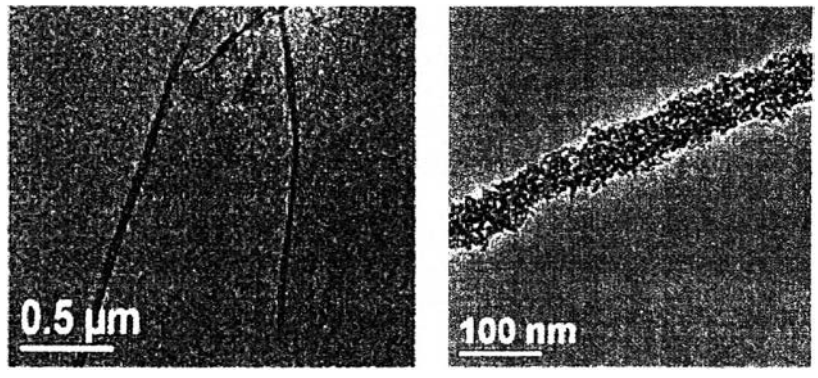

Figure 2.21 Bacterial cellulose/TiO_2 hybrid nanofibers prepared by the surface hydrolysis method with molecular precision.